Effects of Inactivation of the Anterior Interpositus Nucleus on the Kinematic and Dynamic Control of Multijoint Movement

SCOTT E. COOPER, JOHN H. MARTIN, AND CLAUDE GHEZ
Center for Neurobiology and Behavior, Columbia University; and the New York State Psychiatric Institute, New York, New York 10032

Received 16 March 2000; accepted in final form 29 June 2000

Cooper, Scott E., John H. Martin, and Claude Ghez. Effects of inactivation of the anterior interpositus nucleus on the kinematic and dynamic control of multijoint movement. *J Neurophysiol* 84: 1988–2000, 2000. We previously showed that inactivating the anterior interpositus nucleus in cats disrupts prehension; paw paths, normally straight and accurate, become curved, hypometric, and more variable. In the present study, we determined the joint kinematic and dynamic origins of this impairment. Animals were restrained in a hammock and trained to reach and grasp a cube of meat from a narrow food well at varied heights; movements were monitored using the MacReflex analysis system. The anterior interpositus nucleus was inactivated by microinjection of the GABA agonist muscimol (0.25–0.5 μg in 0.5 μL saline). For each joint, we computed the torque due to gravity, inertial resistance (termed self torque), interjoint interactions (termed interaction torque), and the combined effects of active muscle contraction and passive soft tissue stretch (termed generalized muscle torque). Inactivation produced significant reductions in the amplitude, velocity, and acceleration of elbow flexion. However, these movements continued to scale normally with target height. Shoulder extension was reduced by inactivation but wrist angular displacement and velocity were not. Inactivation also produced changes in the temporal coordination between elbow, shoulder, and wrist kinematics. Dynamic analysis showed that elbow flexion both before and during inactivation was produced by the combined action of muscle and interaction torque, but that the timing depended on muscle torque. Elbow interaction and muscle torques were scaled to target height both before and during inactivation. Inactivation produced significant reductions in elbow flexor interaction and muscle torques. The duration of elbow flexor muscle torque was prolonged to compensate for the reduction in flexor interaction torque. Shoulder extension was produced by extensor interaction and muscle torques both before and during inactivation. Inactivation produced a reduction in shoulder extension, primarily by reduced interaction torque, but without compensation. Wrist plantarflexion, which occurred during elbow flexion, was driven by plantarflexor interaction and gravitational torques both before and during inactivation. Muscle torque acted in the opposite direction with a phase lead to restrain the plantarflexor interaction torque. During inactivation, there was a reduction in plantarflexor interaction torque and a loss of the phase lead of the muscle torque. Our findings implicate the C1/C3 anterior interpositus zone of the cerebellum in the anticipatory control of intersegmental dynamics during reaching, which zone is required for coordinating the motions of the shoulder and wrist with those of the elbow. In contrast, this cerebellar zone does not play a role in scaling the movement to match a target.

INTRODUCTION

Cerebellar lesions impair the control of single-joint limb movements, producing systematic errors (e.g., hypometria or hypermetria) and increased variability of performance parameters (e.g., angular displacement) (for review, see Brooks and Thach 1981). However, it is well known that the control of multijoint movement is considerably more impaired (Thach et al. 1992). This disproportionate effect on multijoint movement could reflect cumulative defects at individual joints, as suggested by Holmes (1939), or a specific disorder in interjoint control (Luciani 1915; Thach et al. 1992). A compelling reason why multijoint movements are more impaired is that the mechanics of segmented limbs impose control problems for multijoint movements that have no analogue in single-joint movements; inertial interactions due to motion at other joints produce large torques at each joint. For the endpoint of a multijoint movement to be accurate, limb muscle contraction needs to be adapted to these interaction torques at each joint (Ghez et al. 1996; Hoy et al. 1985; Sainberg et al. 1995; Smith and Zernicke 1987). The cerebellum could play a crucial role in producing control signals that take the various torques into account during movement planning. The study of ataxic reaching in patients by Bastian et al. (1996) suggests an important role for the cerebellum in controlling interaction torques.

We have approached the problem of cerebellar control of multijoint movement by studying the strategies used by cats to perform a prehension task (Cooper 1995; Martin et al. 1995). During performance of this task, we have shown that cats use visuo-spatial information from the target to scale elbow joint excursions and velocity to control reach height, which is similar to multijoint strategies that have been described in other prehension tasks in cats (Perfiliev and Pettersson 1998; Pettersson et al. 1997) as well as in humans (e.g., Jakobson and Goodale 1991; Jeannerod 1984). We have found that this control of scaled elbow excursions is coordinated with motions at the other forelimb joints, which keeps the paw path straight as the limb is lifted to the height of the target (Martin et al. 1995). Straight distal joint and hand paths are general characteristics of reaching in our task as well as reaching in humans (Morasso 1981).

In a previous study (Martin et al. 2000) we showed that inactivating the anterior interpositus nucleus (AIP), which receives the output of the C1-C3 paravermal zones (Trott and

Address for reprint requests: J. H. Martin, Center for Neurobiology and Behavior, Columbia University, 1051 Riverside Dr., New York, NY 10032 (E-mail: jm17@columbia.edu) or S. E. Cooper, Dept. of Neurology, Columbia University, 710 W. 168th St., New York, NY 10032 (E-mail: sec6@columbia.edu).

The costs of publication of this article were defrayed in part by the payment of page charges. The article must therefore be hereby marked "*advertisement*" in accordance with 18 U.S.C. Section 1734 solely to indicate this fact.

Armstrong 1987), impaired performance in this task; paw paths became hypometric and path curvature was increased. The purpose of the present study was to determine the impairments in joint trajectory control that underlie these path defects. Hypometric paw paths could be due to weakness or, alternatively, to a scaling defect in which the transformation from target information to movement parameters is altered. To distinguish these alternatives, it is necessary to study movements to a range of targets. The changes in path curvature produced by AIP inactivation could be due to a failure to control intersegmental interjoint interaction torques during movement, as occurs in human deafferentation (Gordon et al. 1994; Sainberg et al. 1995). Analysis of the temporal variations in joint torques is necessary to distinguish the possible effects of altered neuromuscular control from the effects of biomechanical interactions in inaccurate movements.

To analyze joint torques, we developed a four-segment model of the cat forelimb (Cooper 1995) similar to the three-segment cat hindlimb model of Hoy et al. (1985). These authors expressed limb movement in terms of limb segment angles; we followed instead the convention of Hollerbach and Flash (1982) and used joint angles. Since the nervous system has proprioceptive information about joint motion available to it, but lacks a direct measure of segment angles, we felt that the equations of motion in terms of joint angles would more accurately represent the control problem from the point of view of the brain.

We partitioned torques into three computed components: "interaction" torque, which corresponds to the torque at one joint produced by motion at the other joints; "self" torque, which is an acceleration-dependent torque reflecting inertial resistance; and gravitational torque. The sum of these torques is equal and opposite to a residual term that we refer to as "generalized muscle" torque or "muscle torque." This corresponds to the summed net mechanical contributions of muscle contraction acting at the joint and the "passive" resistance of soft tissue deformation. When the limb is in contact with external objects, muscle torque also includes torque exerted on the limb by those objects (e.g., ground reaction force). We computed those torques to determine the relative contributions of muscle and interaction torques to normal and ataxic movements. We were particularly interested in identifying changes in the way animals used muscle torque to compensate for interaction torque during AIP inactivation.

We began with an analysis of joint kinematics, examining the relations between individual joint angular motions and target height. We next examined the relation of shoulder and wrist motions to those at the elbow, both through kinematic and joint torque analyses. AIP inactivation slowed movements at all joints but did not disrupt the scaling of elbow excursions to the target. Inactivation impaired substantially the anticipatory control of interaction torques at each joint. Some of the results were presented in an abstract (Cooper and Ghez 1991), a doctoral thesis (Cooper 1995), and a review (Ghez et al. 1996).

METHODS

Three cats were used for the kinematic and two for the dynamic analyses of normal and dysmetric reaching during AIP inactivation. These cats were also subjects in our prior study (Martin et al. 2000). All procedures were approved by the New York State Psychiatric Institute Animal Care and Use Committee.

The general methods for behavioral training and testing, data acquisition, basic kinematic analysis, the inactivation procedure, and histological identification have been described in detail (Martin et al. 2000). Here, we briefly summarize the methods. Cats were trained to reach to the back of a narrow food well to grasp a cube of meat (for details see Martin and Ghez 1993; Martin et al. 1995). The food well was instrumented with photocells to detect paw entry. To minimize trial-to-trial variability in the position of the shoulder relative to the food well, cats were restrained in a cloth vest attached to a hammock. Cats were required to stand on narrow supports to minimize paw placement variability at the start of the reach. The forepaw supports were instrumented with a strain gauge for signaling the time when the reaching paw lifted off of the support (toe off). Reaching was elicited during discrete trials that were initiated when the cat placed all four paws on the supports (Martin et al. 1995). After a period of 0.5–1.5 s of stable stance, the animal was permitted to reach to the food well. Trials were run in blocks. In the present study, we present data on reaching to a range of target heights (8, 11, 14, 17, and 20 cm from the foot plate) at a standard anteroposterior location (14 cm forward of the foot plate). Sessions consisted of 100–150 control (i.e., preinjection) trials and 100–300 test or inactivation (i.e., postinjection) trials.

Surgical procedures

Prior to surgery for implanting the chamber, the head fixation device, and the shoulder pin for mounting the elbow and shoulder markers (see *Analysis*), cats received atropine (0.5 mg/kg im) and an antibiotic (benzathine penicillin, 300,000 units im). They were sedated with ketamine (20 mg/kg im) and anesthetized with sodium pentobarbital (30 mg/kg iv). Additional doses of sodium pentobarbital (5 mg iv) were administered as needed. During surgery, lactated Ringer was administered intravenously and body temperature was maintained at 39° with a heating pad. Following surgery, animals received buprenorphine (0.03 mg/kg im) for analgesia. Animals were mounted in a stereotaxic head holder (Kopf Instruments Inc.), a craniotomy was made over the cerebellum ipsilateral to the trained limb, and a chamber was implanted (at 30° posterior angulation) for mounting the recording and inactivation apparatus.

Electrophysiological procedures and reversible inactivation

Sites for nuclear injection were identified by recording the presence of units with large somatic spikes at the appropriate stereotaxic coordinates (for details see Martin et al. 2000). We recorded unit activity in response to skin contact, movement of limb joints, etc., and evoked muscle contraction and joint movement of the contralateral limbs at threshold currents ($<$40 μA threshold, 0.5 MΩ etched tungsten electrode, 330 Hz, 45 ms train, 200 μsec balanced biphasic pulses). Muscimol (0.25–1.0 μg/μL in isotonic saline) microinjections were made using a custom-designed cannula (33 gauge stainless steel hypodermic tubing; for details see Martin and Ghez 1993, 1999) connected to a Hamilton microliter syringe with Teflon or polyethylene tubing. Injected volume was checked by measuring movement of the drug–oil meniscus with a microscope and calibrated graticule. For most injections, we mixed Evans blue dye or fluorescent-labeled latex microspheres with the muscimol solution to mark the injection site for later histological reconstruction.

For muscimol microinjection, the cat's head was mechanically fixed to a rigid support using an implanted device and, by means of a hydraulic microdrive, the cannula was lowered to the injection site. Following a four-minute wait, the solution was injected over a period of 4–6 min. We typically used 0.25–0.5 μg muscimol in 0.5 μL saline. The cannula was left in place after the injection for an additional four minutes, to minimize drug spread, and was then withdrawn. The cat's head was then released from fixation and behavioral testing resumed. The total delay between control and postinjection testing was 15–20 min; the delay between the start of injection and resumption of behavioral testing was no more than 12 min. Behavioral

testing after injection lasted one hour or less. We made muscimol injections adjacent to (i.e., within 1 or 2 mm) the AIP inactivation sites (posterior interpositus, fastigial nucleus, white matter) to verify the specificity of effects (see Martin et al. 2000).

At the conclusion of experiments, we made electrolytic marking lesions (10 μA $\times$ 15 s, 0.5 MΩ etched tungsten microelectrode) (see also Martin et al. 2000). Cats were administered a lethal dose of pentobarbital sodium and perfused through the left ventricle with saline followed by 4% paraformaldehyde solution. The brain was stereotactically blocked in situ, postfixed, and cryoprotected. Frozen sections (40 μm) were cut parasagittally or in a coronal plane with the same posterior angulation (30°) as the injection cannulae. Even-numbered sections were mounted unstained for fluorescence microscopy of the microspheres and odd-numbered sections were processed using either Nissl-myelin (Klüver-Barrera) or plain Nissl methods. Injection sites were reconstructed and nuclear boundaries were drawn in accordance with cytoarchitectonic criteria (Berman 1968; Berntson et al. 1978). These AIP injection sites corresponded to those presented in our previous report (Martin et al. 2000).

Analysis

We used the MacReflex motion analysis system (Qualisys, Inc.) for the kinematic and dynamic analysis of reaching (Martin et al. 1995, 2000). Markers were placed directly on the lateral surface of the distal phalanx of the fourth digit (paw tip), on the skin directly over the metacarpalphalangeal (MCP) joint of the fifth digit, and on the styloid process of the ulna (wrist joint). To accurately monitor shoulder and elbow joint locations, since the skin slides over the shoulder and elbow joints during forelimb motion, we implanted an orthopedic pin through the bone of the greater tuberosity of the humerus and into the medullary cavity prior to behavioral training. The pin protruded 1 cm from the skin surface to provide a stable attachment site for a light-weight metal rod on which markers corresponding to the shoulder and elbow joints were mounted (see *Surgical procedures* for general surgical procedure; see Martin et al. 1995 for details). The MacReflex cameras were controlled with National Instruments TTL I/O hardware and custom software. Force plate and photocell signals were acquired at 100 Hz using 16-bit A/D converters (Macintosh II computer with National Instruments I/O and DMA boards) synchronized with the video cameras by the software. Joint and paw-tip *x-y* coordinates, sampled at 100 Hz, were computed and analyzed with custom software written in Matlab programming language. Upper arm, forearm, and metacarpal limb segments were defined as joining the shoulder, elbow, wrist, and MCP joints. The most distal part of the limb was treated as a single phalangeal segment joining the MCP and the paw tip. Shoulder angle was computed as the angle between the arm segment and the horizontal plane (see Fig. 1, *inset*).

Elbow angle was computed as the angle between the arm and forearm segments, wrist angle as the angle between the forearm and metacarpal segments, and MCP as the angle between the metacarpal segment and the tip of the fourth digit. Time derivatives (e.g., joint angular velocities) were computed with a three-point central difference filter and accelerations were computed by differentiating twice. For the ensemble averages shown in Fig. 1, trials were aligned on the time at which the wrist speed crossed a threshold of 10% of its peak value on that trial. This criterion was chosen empirically as representing the earliest reliably detectable movement at the beginning of the reach. A percentage of peak rather than an absolute level was chosen to avoid an artifactual delay in onset for slower movements. For the ensemble averages of torque data (and associated kinematic data) shown in Figs. 4, 5, and 8, trials were aligned with the time the paw broke contact with the force plate on which it rested. Toe off has the disadvantage of occurring later in the movement than the 10% peak wrist speed, but we used it for the dynamic analysis because it demarcates the portion of the movement where generalized muscle torque excludes ground reaction force.

Amplitudes and the times of occurrence of peaks (local maxima and minima) and onsets in time series of individual trials were measured by operator-assisted custom Matlab software routines. To avoid a bias toward underestimating the amplitude of narrow peaks, a second-order polynomial was fit to the three samples spanning the maximum (or minimum) sample value and the maximum (or minimum) of the polynomial determined.

Onset and peak data for both kinematic and torque data were assembled into two multi-experiment databases, one for target-height variations in normal cats, which contained 714 reaching movements, and another for inactivation, which contained 1,957 reaching movements to various target heights before and after muscimol injection. Statistical analysis of these databases was done using the programs Statview 4 and Super ANOVA. For tests of significance, we used a least-squares general linear model

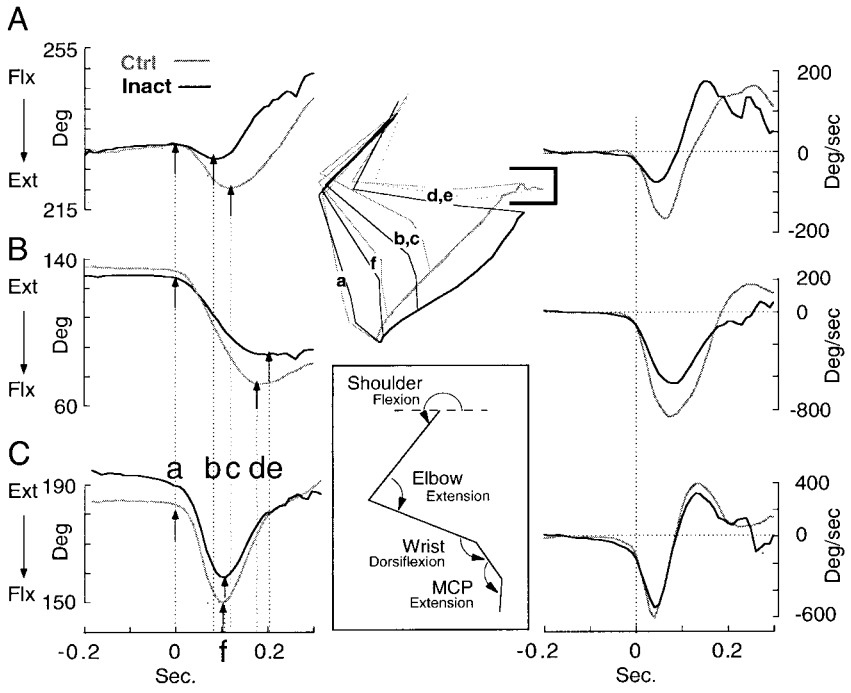

FIG. 1. Ensemble averages of shoulder (*A*), elbow (*B*), and wrist (*C*) joint angles (*left*) and angular velocities (*right*) for reaches to a standard height (14 cm) and distance (11 cm). Gray lines, preinjection control reaches; black lines, postinjection reaches. Averages synchronized with wrist speed onset (see METHODS). *Top inset*: stick figures at four sequential times during representative single control (gray) and test (black) reaches. a, movement onset; f, peak wrist flexor joint angle; b, control and c, test peak shoulder extensor joint angles; d, control and e, test peak elbow extensor joint angles. *Bottom inset*: joint angle conventions (n = 22 before inactivation and 32 during inactivation).

$$Y = K + \text{Expt} + \text{TDV} + \text{Inact} + \text{Inact} \times \text{TDV}$$

where K = constant, Expt = experiment number, TDV = target dorsoventral position, and Inact = 1 during inactivation, 0 as control.

Dynamic analysis

Equations of motion for a four-segment planar limb are given in the APPENDIX. These expressions describe the torque required at a given joint to produce a particular pattern of limb motion. Equivalently, they describe a motion-dependent torque at that segment that must be overcome by muscle contraction, tendon stretch, etc. (d'Alembert's principle) (Cooper 1995). We partitioned the biomechanical effects in the equation of motion (see APPENDIX) into three components: self, interaction, and gravitational torques. Muscle torque is defined as equal and opposite to the sum of the other three torques and includes the net mechanical contribution of muscle contraction acting at the joint. It also includes the "passive" resistance of soft tissue deformation and, at the beginning and end of movement, contact with external objects (e.g., ground reaction forces prior to the time the paw broke contact with the force plate). As discussed in the INTRODUCTION (see also APPENDIX), we follow the convention of Hollerbach and Flash (1982) and use *joint* angles for describing torques.

Because we are interested in the problem of interjoint coordination when movements at one joint produce torque at another joint, we chose a form for the equations that distinguishes *self* torque, which we define as torque at a joint related only to movement at that joint, from *interaction* torque, defined as torque at a joint caused by the movement of *other* joints (itself due in part to the contraction of muscles at those joints). As in the two-joint model of Hollerbach and Flash (1982), the terms of the expression include *acceleration-dependent* torques (proportional to $\ddot{\Theta}_i$), *centrifugal* torques (proportional to $\dot{\Theta}_i^2$), and *Coriolis* torques (proportional to $\dot{\Theta}_i\dot{\Theta}_k$, $i \neq k$). For a given joint i, the $\ddot{\Theta}_i$ term is the only one not dependent on motions of joints other than i and so represents the self torque (i.e., inertial resistance to motion). Interaction torque is the sum of all the other terms. Note that interaction torque includes two additional terms proportional to the x and y components of *linear* acceleration at the most proximal joint. This represents the lumped effect of all the joints in a cat's body proximal to the shoulder and is included for completeness. In these experiments, animals were restrained in a hammock, which minimized this lumped joint effect. Since in the present research we studied limb movements in a vertical plane, we included a term for torque due to gravity; this term is identical to the y-double-dot term, with y-double-dot equal to gravitational acceleration $g = 9.8$ m/s^2. Values for limb segment moments of inertia, masses, lengths, and the locations of segment centers of mass were estimated individually for each cat from published regression equations (Hoy and Zernicke 1985). We validated the programs by comparing the generalized muscle torque they computed from experimental data with that computed by a completely independent method (the free-body method) (Cooper 1995).

For computation of torques, joint angles were defined as follows. The proximal segment was extended distally past the joint and an angle was measured counterclockwise from the extension to the next segment (see Fig. 1, *inset*). A consequence of this convention is that positive torques correspond to flexion at the shoulder and elbow but dorsiflexion at the wrist.

RESULTS

Kinematics of dysmetric movements: hypometria and impaired interjoint coordination

ELBOW AND SHOULDER MOTIONS. The intact cat reaches for targets located over most of the workspace by scaling the elbow displacement and velocity to target height. Shoulder motion, which initially extends during lift to retract the paw and later flexes to protract the paw, exhibits a more complex dependency on target location (Martin et al. 1995). As shown in Fig. 1, both elbow flexion and shoulder extension were reduced in speed and amplitude by AIP inactivation. Figure 2, which presents grouped data from 15 sessions in three cats, shows that AIP inactivation did not alter the dependency of these quantities on target height although, on average, elbow flexor velocity was reduced by 30% and shoulder extensions by 54%. While elbow flexion remained hypometric during inactivation for all target heights, peak angle and angular velocities were related to target height (main effect of inactivation on peak elbow angle and peak elbow angular velocity significant at $P \leq 0.0001$). Inactivation had no effect on this relationship. Inactivation also produced a reduction in shoulder extension and velocity (main effect on peak angle and angular velocity significant at $P \leq 0.0001$). Thus hypometria did not result from a change in the strategy normally used for scaling joint trajectories with targets at different heights.

The ensemble averages in Fig. 1 show differences in the time course of both elbow and shoulder movement during AIP inactivation; whereas the shoulder extensor phase was reduced in duration (Fig. 1, *left*; control, a–b interval; inactivation, a–c interval), elbow flexion was prolonged (Fig. 1; control, a–d interval; inactivation, a–e interval). Normally, the shoulder and elbow reversals were nearly synchronous (Fig. 3, open histogram). During inactivation, the mean interval from shoulder to elbow reversal increased as did its variability (20 ± 12 to 42 ± 37 ms; $P < 0.001$; Fig. 3, filled histogram; see also Fig. 1, *left*; control, c–d interval; inactivation, b–e interval).

In both normal and inactivated conditions, as target height was increased, shoulder reversal from extension to flexion occurred at increasingly flexed elbow angles. Since the elbow flexion varied with both target height and inactivation state, we

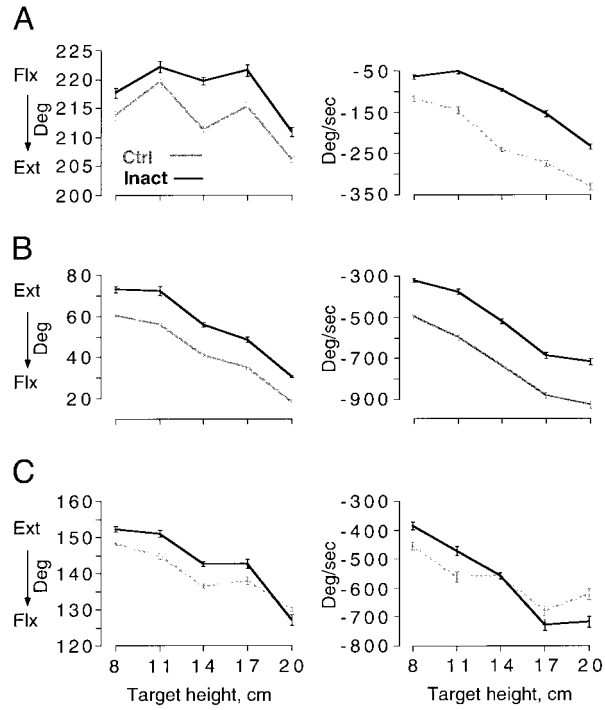

FIG. 2. Relation between kinematic changes at the shoulder (*A*), elbow (*B*), and wrist (*C*) before (gray lines) and during (black lines) inactivation. *Left*: changes in peak shoulder extensor, elbow flexor, and wrist flexor joint angles. *Right*: angular velocity for the joint angles shown at *left*.

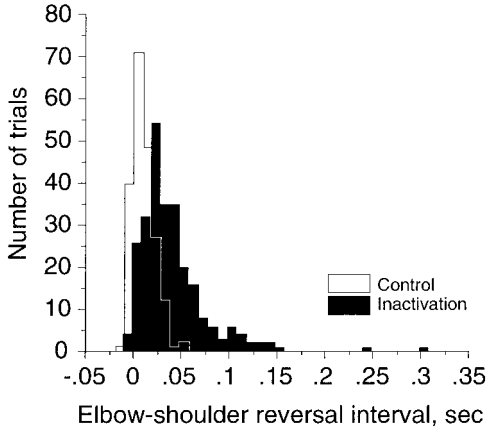

FIG. 3. Histograms showing the distribution of the interval between peak elbow flexor velocity and peak shoulder extensor velocity for control (white) and inactivation (black) trials. Data presented for standard target from 8 sessions in 2 cats ($n = 203$ before inactivation and 286 during inactivation).

calculated the fraction of the maximal elbow excursion when shoulder joint angle reversed from extension to flexion. For control reaches, such reversal in shoulder angle occurred at 79% of maximal elbow flexion, independent of target height ($r = 0.003$; not significant). During AIP inactivation, reversal occurred significantly earlier at 54% of maximal elbow flexion ($P < 0.0001$). The reduction in shoulder extension, which retracts the paw early during lift, with relative preservation in shoulder flexion causes the paw to ultimately collide with the undersurface of the target.

WRIST MOTIONS. As can be seen in Fig. 1*C* for both the control and inactivated conditions, the wrist undergoes an initial plantar flexion as the paw is lifted from the ground and a later dorsiflexion of approximately equal magnitude as it approaches the food well. Also during both control and inactivation, plantarflexion and dorsiflexion increase with the height of the target (Fig. 2*C*, *left*, plantar flexion shown). The slope of the relation of wrist plantarflexor velocity and target height *increased* during AIP inactivation (Fig. 2*C*, *right*). The same appeared to be true of dorsiflexion, but this was difficult to verify statistically since the paw often collided with the food well before peak dorsiflexor velocity occurred.

Along with the increased dependence of wrist flexor velocity on target height, there was a systematic change in the timing of the wrist plantarflexion-dorsiflexion reversal (i.e., wrist flexion to extension) relative to elbow flexion across target heights. During preinjection control trials, as animals reached to higher targets, the wrist reversed direction progressively later in the reach (i.e., at elbow angles that were increasingly flexed). During AIP inactivation, wrist reversal occurred prematurely. Computation of the fraction of elbow flexion completed at the time of wrist reversal showed that, like as for the shoulder, it occurred at a decreased fraction of peak elbow flexion (65% vs. 54%; $P = 0.0001$). Kinematic changes at the wrist during inactivation, as with the shoulder, contributed to bowing of the paw path.

Dynamics of dysmetric movements: impairments in anticipatory control of interaction torques

As noted earlier, for multijoint movements to be accurate, muscle contraction needs to be adapted to the complex, time-varying, inertial interaction and gravitational torques acting at each joint (Ghez et al. 1996; Hoy et al. 1985; Sainberg et al. 1995; Smith and Zernicke 1987). Analysis of the temporal variations in joint torques is therefore necessary to distinguish possible effects of altered neuromuscular control from effects of biomechanical interactions in causing movements to be inaccurate.

SHOULDER DYNAMICS. *Normal.* Figure 4 shows ensemble averages of shoulder kinematics (*top*) and joint torques (*bottom*) for a single representative experiment (*left*, control trials; *right*, trials during inactivation). Shoulder muscle torque shows a constant extensor bias, which counters the flexor gravitational torque present throughout the movement. Superimposed on this are phasic extensor muscle and interaction torques, which produce the observed shoulder extension (Fig. 4, *left*). Because the mass and length of the paw were small, the major determinant of the shoulder extensor interaction torque was the acceleration of the elbow into flexion. The temporal variation in muscle torque paralleled changes in acceleration, which is expected if shoulder muscles contribute to shoulder acceleration. More surprisingly, the timing of changes in interaction torque *also* paralleled shoulder acceleration; the reversal in shoulder angular acceleration, from extension to flexion (Fig. 4, arrow), was coincident with the reversal in interaction torque and the subsequent peak flexor acceleration and also coincident with the peak interaction torque (Fig. 4). While muscle and interaction torque were similar in their relation to acceleration, they differed in their magnitudes; the extensor peak of muscle torque was consistently smaller and frequently more indistinct than that of interaction torque and was not seen at every target height in every experiment. The extensor peak of interaction torque, on the other hand, was recognizable at all target heights

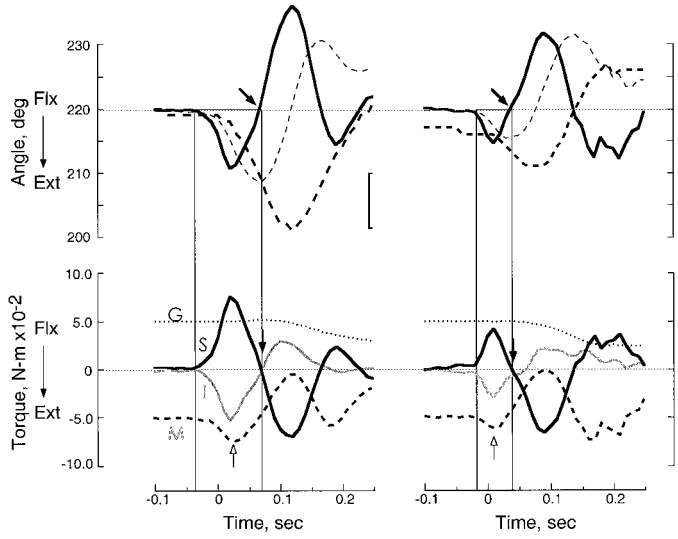

FIG. 4. Ensemble averages of measured joint angle and computed joint torques at the shoulder for reaches during the control (*left*) and inactivation (*right*) periods. *Top*: ensemble averages of shoulder joint angle (thick dashed line), angular velocity (thin dashed line), and acceleration (solid line). *Bottom*: ensemble averages of gravitation (dotted line), muscle (dashed line), interaction (gray line), and self (solid line) torques. All averages are synchronized with the time the paw breaks contact with the force plate (i.e., toe off). Arrows: reversal from extensor to flexor acceleration (*top*) and flexor to extensor self torque (and extensor to flexor interaction torque) (*bottom*). Open arrow: peak extensor muscle torque. Thin vertical lines: acceleration onset (*left*) and reversal from the extensor to flexor phases of shoulder acceleration (*right*). I, interaction torque; M, muscle torque; G, gravitational torque; S, self torque ($n = 20$ before inactivation and 27 during inactivation). Calibration: 4000 deg/s/s; 200 deg/s.

and in every experiment. Interaction and muscle torques acted together to overcome inertial resistance (i.e., self torque) and gravity to accelerate the shoulder into extension. However, since the extensor interaction torque was larger than the phasic extensor component of muscle torque, interaction torque contributed as much or more than muscle torque to shoulder extension.

AIP inactivation. As noted earlier, the main kinematic effect of AIP inactivation at the shoulder was a pronounced decrease in amplitude, speed, and duration of the initial extension. Figure 4 (*right*) shows that both peak muscle and interaction torques were substantially reduced (open arrows). Significant decreases were present across all experiments ($P < 0.001$). The intervals between the peaks in interaction and muscle torques were unchanged during AIP inactivation. These findings suggest that the reduction in interaction torque was an important cause of the reduction in shoulder extension since this torque was the major determinant of this phase of motion.

ELBOW DYNAMICS. *Normal.* Like the initial shoulder extension, flexion of the elbow resulted from the combined effects of muscle and interaction torque, which overcame the extensor actions of gravity and inertia (i.e., gravitational and self torque). As Fig. 5 (*left*) shows, acceleration and interaction torques peaked at the same time. However, unlike at the shoulder, where muscle and interaction torques changed in parallel throughout the movement, elbow muscle torque remained flexor and continued to rise while interaction torque reversed from flexion into extension. Thus elbow flexor acceleration was prolonged past the end of flexor interaction torque by a prolonged muscle torque. The continued rise in muscle torque after the reversal of interaction torque into extension was a consistent feature of movements to targets in all locations. It can also be seen in Fig. 5 (*left*) that the transition from elbow flexor to extensor acceleration (*right vertical line*) occurred just after the peak in muscle torque but well after the transition to extensor interaction torque. Thus the timing of the direction reversal at the elbow, unlike that at the shoulder, appeared to be dependent on changes in elbow muscle torque. At this point in the movement, the elbow was in the middle of its range of motion, where stretch of muscle viscoelastic elements is less than at the extremes of joint motion and where the paw is not in contact with external objects. At this transition, the component of muscle torque caused by passive muscle stretch is least and the component caused by active muscle contraction is greatest. Thus at elbow reversal, elbow muscle torque is likely to be dominated by active muscle contraction. Taken together with the above observations on the relative timing of elbow acceleration and elbow muscle torque, this suggests that reversal in elbow acceleration reflects the timing of active muscle contraction.

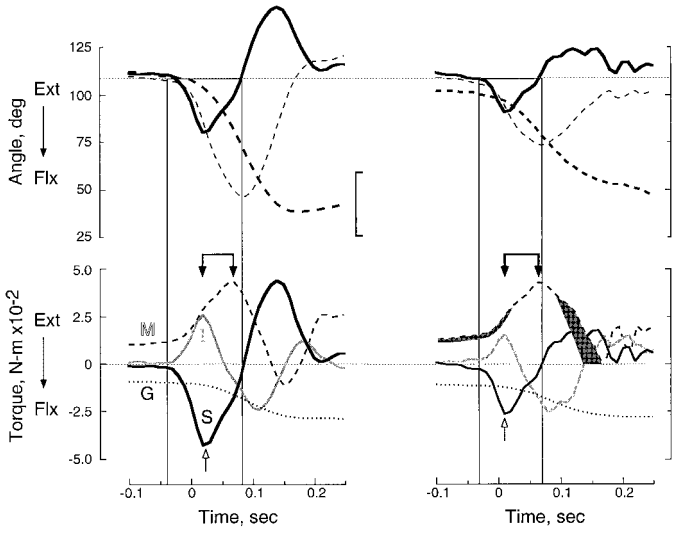

FIG. 5. Ensemble averages of measured joint angle and computed joint torques at the elbow for reaches during the control (*left*) and inactivation (*right*) periods. Same format as Fig. 4. Brackets with filled arrowheads: interval between peak flexor interaction torque and peak flexor muscle torque. Open arrow: peak extensor self torque. Gray shaded region (*right*) identifies difference between average muscle torque prior to and during inactivation. Average during inactivation is primarily prolonged. Thin vertical lines: acceleration onset (*left*) and reversal from the flexor to extensor phases of the elbow acceleration (*right*) ($n = 20$ before inactivation and 27 during inactivation) Calibration: −10000 deg/s/s; −400 deg/s.

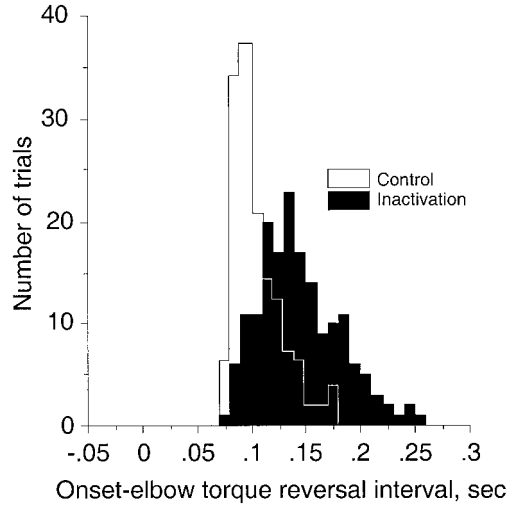

FIG. 6. Histograms showing that reversal from elbow flexor to extensor muscle torque is prolonged during anterior interpositus nucleus (AIP) inactivation. Data for reaches to standard target height and distance from 6 sessions in 2 cats. Open histogram: preinjection control reaches (mean = 101 ± 23 ms; $n = 142$); closed histogram: postinjection test reaches (mean = 144 ± 53; $n = 173$).

AIP inactivation. The data in Fig. 5 (*right*) show a substantial reduction in elbow flexor interaction torque during inactivation. Although the amplitude of the elbow flexor muscle torque was similar to controls, its duration was clearly increased (dark gray area). Across cats, interaction torque was reduced 47% on average ($P < 0.0001$) whereas peak muscle torque was reduced only slightly (6%; $P = 0.039$). In contrast to this relatively unchanged amplitude, the duration of the flexor muscle torque increased. The time from movement onset to reversal from flexor to extensor muscle torque increased from 101 ± 2 to 144 ± 4 ms ($P < 0.0001$) (Fig. 6). This prolongation occurred disproportionately as flexor muscle torque was declining (10 ms increase in the time from movement onset to peak as compared with 33 ms increase in the time from peak to zero cross; both significant at $P < 0.001$). The prolongation in flexor muscle torque resulted in a significant increase in the duration of elbow flexion (see Fig. 7*D*) and acted to bring the paw farther toward the food well. Thus it could reflect a compensatory adjustment for the reduced muscle and interaction torques.

Figure 7 shows that the increase in peak velocity that occurred with reaches to higher targets (*A*) was associated with

increases in muscle and interaction torques both before and during inactivation (*B* and *C*; similar to Fig. 2). Figure 7*D* also shows that the duration of flexion did not vary systematically with target height but was increased overall during inactivation. This shows that the strategy for controlling the height of the movement using a scaled command for elbow flexion remained unimpaired.

WRIST DYNAMICS. *Normal.* We saw earlier (Fig. 1*C*) that the wrist underwent a biphasic sequence of plantar- and dorsiflexor motions. Figure 8 (*left*) shows that the initial plantarflexor acceleration was driven by changes in interaction and gravitational torques acting in the same plantarflexor direction. Muscle torque was in the direction opposite to the acceleration for most of the reach and therefore restrained wrist motion. The reversal into dorsiflexion occurred once the plantarflexor interaction torque began to decline from its maximal value. Peak dorsiflexor acceleration occurred during the brief interval when interaction and muscle torques were both in the same (dorsiflexor) direction. This synergy was a consistent feature of ensemble averages of wrist torques in all experiments and is shown by the shaded region in Fig. 8. The timing of reversal from plantar- to dorsiflexion was determined by the interaction torque and the peak dorsiflexion was determined by the synergy between interaction and muscle torques.

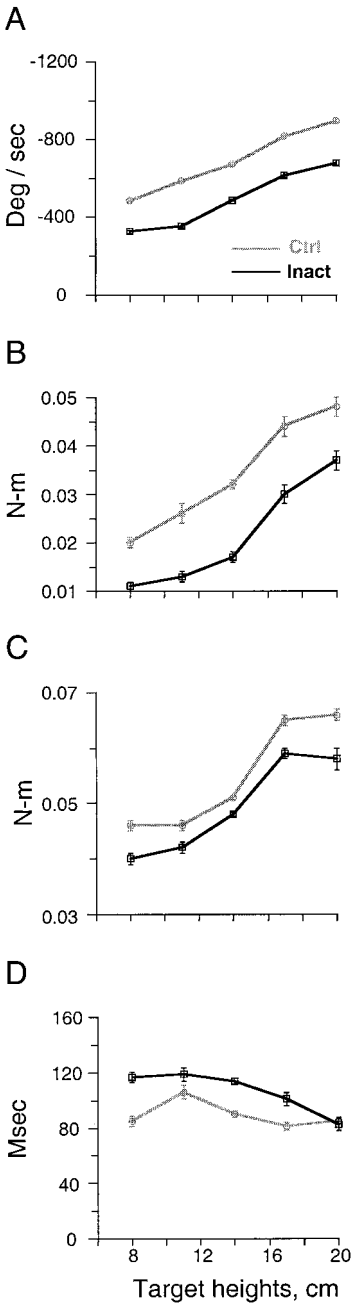

FIG. 7. Scaling of elbow torques for reaches to higher targets before (gray lines) and during (black lines) inactivation. *A*: elbow velocity. Data replotted from Fig. 2*B*, *right*, but the *y* scale is inverted to show the same trend as in parts *B* and *C*. *B*: elbow interaction torque; *C*: elbow muscle torque; *D*: time to peak elbow joint angular velocity. Data are from 8 sessions in 2 cats.

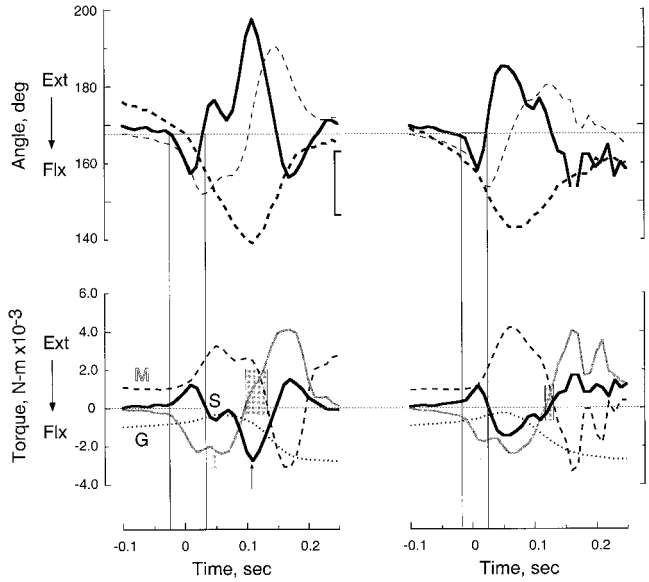

FIG. 8. Ensemble averages of measured joint angle and computed joint torques at the wrist for reaches during control (*left*) and inactivation (*right*) periods. Same format as Figs. 4 and 5. Note that the gravitational torque remains flexor during the flexor and extensor phases of movement. Shaded regions, *bottom*: period of overlap between extensor muscle torque and extensor interaction torque. Thin vertical lines: acceleration onset (*left*) and reversal from the plantar flexor to dorsiflexor phases of wrist acceleration (*right*) (n = 21 before inactivation and 27 during inactivation). Calibration: −10000 deg/s/s; −400 deg/s.

AIP inactivation. As noted earlier (see *Kinematics of dysmetric movements.* WRIST MOTIONS; Fig. 1*C*), wrist plantarflexor velocity showed no overall change with inactivation; however, its dependence on target height increased. The initial acceleration was significantly reduced in magnitude by 30% overall ($P < 0.0001$). As can be seen in Fig. 8 (*right*), the wrist reversal and the subsequent peak dorsiflexor acceleration occurred earlier than in control animals. Overall, the reduction in acceleration was mainly due to a 33% ($P < 0.0001$) reduction in plantarflexor interaction torque although, in one of the cats, there also was a small (10%) increase in dorsiflexor muscle torque (Fig. 8). Although the plantarflexor interaction torque driving the initial motion of the wrist was reduced overall, it remained in the flexor direction for a longer duration than in controls. (This would be expected if wrist interaction torque was dominated by torque arising at the elbow, which is probably the case given that angular velocities and accelerations were much greater at the elbow than at the shoulder and that the moment of inertia of the phalangeal limb segment was small relative to the paw.) This effect was shown by the time of reversal from flexor to extensor interaction torque, which was significantly delayed by 27% ($P < 0.0001$) during AIP inactiva-

tion. As noted in the preceding paragraph, dorsiflexor acceleration peaked in the normal cat when the interaction and muscle torques cooperated to produce dorsiflexion (Fig. 8, *left*, boxed region). During AIP inactivation, there was less cooperation between interaction and muscle torques and this reduced the dorsiflexor acceleration. Indeed, in the averages of Fig. 8, the peak plantarflexor interaction torque occurred near the peak dorsiflexor acceleration. In sum, the changes in wrist kinematics reflected both wrist muscle torque and interaction torque.

These changes in wrist dynamics can be explained by a change in the relative contributions of active and passive components of muscle torque. To see how this is so, it should be recalled that after toe off, ground reaction force no longer contributes to muscle torque, which is then composed only of active muscle contraction plus passive viscoelastic torques. We found that, prior to inactivation, wrist dorsiflexor muscle torque peaked well before the wrist was maximally plantarflexed (Fig. 8, *left*). During inactivation, on the other hand, the two torques reached their peak values simultaneously (Fig. 8, *right*). This suggests that wrist extensor muscle contraction normally contributes substantially to the resistance of the plantarflexion interaction torque that drives the movement. During inactivation, the synchronization of peak muscle torque and joint angle suggests that that simple elastic restoring forces dominated the variations in muscle torque. We examined this relationship further with the analysis shown in Fig. 9.

Figure 9*A* plots plantarflexor interaction torque in relation to target height. For both control and inactivation trials, interaction torque increases with increasing target height, although torque magnitude is less during inactivation. Figure 9*B* plots the interval between peak wrist angle and peak muscle torque. In control reaches (gray), the lead of peak dorsiflexor muscle torque increased with target height. This increasing lead time could reflect the progressively greater contributions of anticipatory muscle contraction that are needed to compensate for increasing flexor interaction torque (Ghez et al. 1996). During inactivation, despite the continued presence of the strong relationship between interaction torque and target height (Fig. 9*A*, black symbols), timing remained invariant, which suggests loss of anticipatory control. Figure 9*C* illustrates wrist muscle torque–wrist joint angle plots for movements to a standard target. Control reaches (*C1*) showed more hysteresis before than during inactivation (*C2*), when the torque–angle relation resembled that of a linear elasticity. These results suggest that during normal reaches, where there is a phase lead of muscle torque over joint angle, the cat exploits interaction torque and dorsiflexes the wrist during a narrow time interval. During AIP inactivation, the wrist behaves more like a passive spring and interaction torque does not contribute to controlling the timing of wrist dorsiflexion.

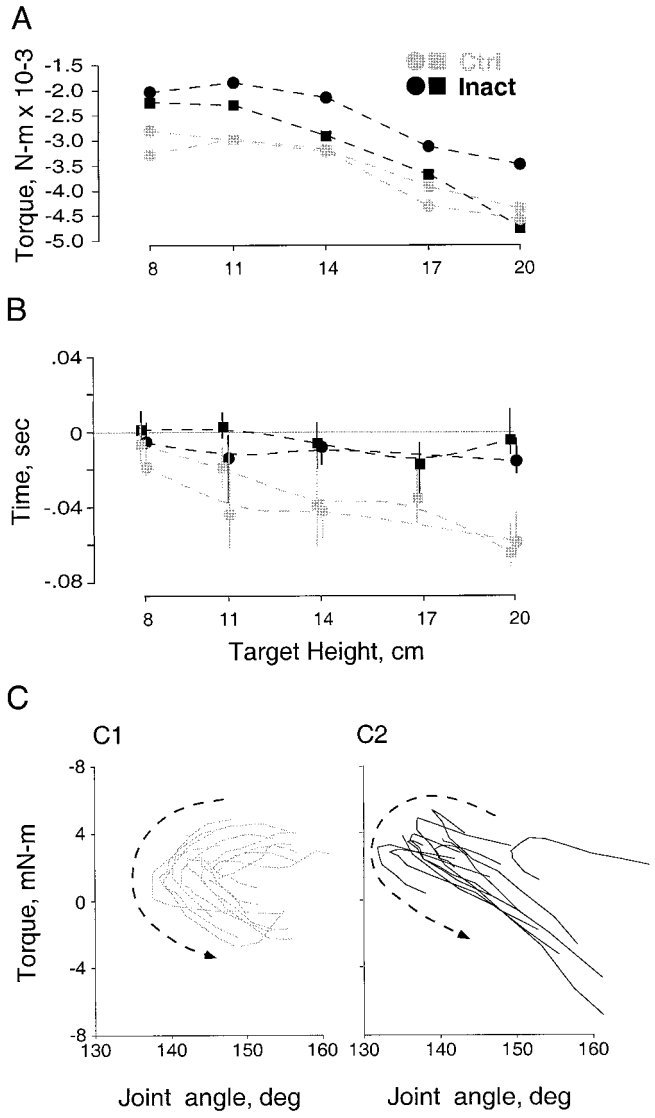

FIG. 9. *A*: relation of peak wrist plantarflexor interaction torque to target height. Data from peak of ensemble averages, aligned on toe off. Data from 2 cats are plotted separately (circles and squares). *B*: relation between lead of peak wrist extensor muscle torque over peak wrist flexor angle as a function of target heights in 2 cats. Mean ± SE of peaks in individual trials. Data in *A* and *B* are from all sessions of two cats, which are plotted separately (circles and squares). Data in *B* are staggered slightly on the *x* axis for clarity. *C*: relationship between wrist muscle torque and joint angle for control (*C1*) and postinjection (*C2*) reaches. Data in *C* are from a single representative session. Dashed arrow: the beginning to the end of the reach.

DISCUSSION

Our analysis of the motions and torques at individual joints during reaching in the cat demonstrates the complexity of the task faced by the nervous system in multijoint control. Moving a single joint requires primarily accelerating a load against the opposing forces of inertia, gravity, and viscoelastic soft tissue elements. The presence of multiple linked segments introduces significant complications because motions at each joint produce torques that act at the other joints (Hollerbach and Flash 1982). These interjoint interaction torques can assist or resist the torque generated by active muscle contraction so that changes in the former must be compensated by the latter. Thus, in producing a desired paw or hand trajectory, neuromuscular control has to be precisely choreographed with time-varying torques generated by other joints. While accuracy in rapid single-joint torques and movements may require that the nervous system develop an internal model of the musculoskeletal system to program appropriate feedforward commands, with multijoint movement such models would need to be much more complex (Wolpert et al. 1995).

Our results show that during AIP inactivation, the linear scaling of kinematic and dynamic parameters to target height was maintained. While decomposition of joint torques into separate components (Cooper 1995) showed that the particular

dynamic control impairments produced by AIP inactivation differed at each joint, there were two common defects. First, there was a systematic reduction in initial acceleration and muscle torque at elbow and shoulder and decreased anticipatory muscle torque at the wrist, consistent with disfacilitation of the cerebellar efferent targets (see *Impaired single and multijoint control produced by AIP inactivation*). Second, there were errors at the beginning of movement and also later, in the adjustments made to correct the initial errors, which suggests that both feedforward and feedback control were affected. Our analysis revealed a lack of compensation for intersegmental interactions similar to that seen in human deafferentation (Ghez et al. 1995; Gordon et al. 1995). We argue below (see *Impaired single and multijoint control produced by AIP inactivation*) that the lack of compensation was due to impaired use of somesthetic feedback in generating or updating internal models of limb dynamics.

Relation of muscle torque to interaction torque at different joints

At the beginning of movement, there were phasic changes in muscle and interaction torque at each joint that overcame inertial resistance (i.e., self torque). Thus neuromuscular control produced movement in two ways: directly, by acting on the joint(s) spanned by the muscle, and indirectly, by producing interaction torques acting at other joints. Decomposition of joint torques (Cooper 1995) revealed qualitative differences in the roles of muscle and interaction torques during reaching at shoulder, elbow, and wrist. At the elbow, while interaction torque assisted elbow flexion, the amplitude and exact timing of elbow flexion, and its compensation for initial hypometria during AIP inactivation (e.g., Fig. 5), was accomplished by muscle torque. Since this prolongation occurred in mid-reach, when the elbow was in the middle of its range of motion and the paw was not in contact with external objects, muscle torque here would have reflected mostly active muscle contraction.

At the shoulder, the phasic increase in extensor muscle torque was smaller than that of interaction torque and the two were not temporally independent. This suggests that control of shoulder muscles during reaching was dominated by the movement of other joints rather than a stimulus-response transformation for scaling reach height to target height. We have shown (Martin et al. 1995) that movements at the shoulder (and wrist) of the reaching limb are not part of the scaling strategy for controlling the height of the reach but that they operate primarily to linearize the paw path. AIP inactivation disturbed this control resulting in bowing of the paw paths.

At the wrist, a third situation prevailed. Here, muscle torque opposed interaction torque for much of the reach. Even without formal dynamic analysis, it can be appreciated that elbow flexor acceleration followed by deceleration produces a plantarflexor/dorsiflexor "whipping" torque at the wrist (Hollerbach and Flash 1982; Smith and Zernicke 1987). This explains why, among the joints we studied, the wrist alone was not slowed during AIP inactivation. Since wrist motions were resisted rather than produced by muscle contractions, reduction in active muscle contraction by inactivation did not result in slowing as at other joints. As expected in such a situation, the slope of the relationship between wrist plantarflexor velocity and target height actually increased during AIP inactivation.

In the normal cat, wrist muscle torque provided phase-advanced damping of passive wrist motion during reaching and could represent feedforward control (Miall 1998) of wrist muscles, based on anticipation of upcoming interaction torques. Alternatively, it could represent viscous resistance in wrist muscles. However, such viscosity cannot be a purely passive property of muscle but rather an effect that was actively regulated by the CNS, since it was disrupted by cerebellar inactivation.

Impaired single and multijoint control produced by AIP inactivation

Our dynamic analysis indicates that AIP inactivation resulted in a reduction in the muscle torque providing the initial angular acceleration at all joints. These reductions are consistent with disfacilitation of cervical spinal motor neuronal pools through the known projections of AIP to magnocellular red nucleus (Robinson et al. 1987) and through projections via ventrolateral thalamus (Anderson and DeVito 1987) to primary motor cortex (Jörntell and Ekerot 1999). Three reasons indicate that this reduced muscle activation did not reflect simple weakness (i.e., an absolute limitation on the capacity for generating force) over the range studied. First, preservation of scaling and elbow flexor muscle torque compensation indicated that there was a capacity for increasing muscle force. Second, the animals' paws struck the outside of the food well. Had the well not been there, the paw would have passed through the location of the bait; clearly, muscle contractions were adequate to carry the paw to the desired endpoint. Third, the animals were able to extend their shoulder to withdraw the limb and replace it in the food well after contacting the underside of the well. This is similar to our previous finding that, during AIP inactivation, animals could extend the shoulder sufficiently to reach over an obstacle after bumping into it (Martin et al. 2000). However, as in the previous study, the animals were not able to generate sufficient muscle force in an anticipatory, feedforward manner.

Dynamic analyses revealed that the reductions in elbow flexion and shoulder extension were also due to decreases in interaction torque. At both the elbow and shoulder, there was a failure of initial muscle torque to take into account the reductions in interaction torque. At the elbow, compensation for reach height did take place by prolonging the initially hypometric flexion. That duration, rather than amplitude, was adjusted suggests that compensation was accomplished by a feedback mechanism. This is supported by the observation that most of the prolongation took place during the latter half of the movement (~120 ms or more after movement onset; Fig. 5, *right*; muscle torque, gray area), allowing time for transmission of information around a feedback loop. This latency corresponds to a visual reaction time in the cat (Ghez and Vicario 1978) and is consistent with the hypothesis that the compensation was based on visual feedback. This compensation, however, failed to produce an accurate reach because there was no corresponding increase in extensor muscle torque at the shoulder, which would have been needed to prevent the paw from colliding with the underside of the food well. The reach remained inaccurate because compensation was applied only to scaling and not to control of intersegmental dynamics.

At the wrist, anticipatory control of the plantarflexor interaction torque appeared to be lacking during inactivation because muscle torque behaved like a passive (approximately linear) spring, probably reflecting stretch of passive elastic

joint elements. This breakdown in compensation for interaction torque is similar to the defect in ataxic reaching reported by Bastian et al. (1996) in their patients with cerebellar lesions. However, because those experiments were done in humans, lesions were not confined to a single cerebellar nucleus. A similar lack of compensation may have occurred in the study of Milak et al. (1997). These authors reversibly inactivated the interpositus (though without selectively inactivating the anterior interpositus nucleus vs. the posterior interpositus nucleus) in cats performing a reaching task similar to ours. Although they did not explicitly compute joint torques, they made the intriguing observation that limb kinematics during inactivation resembled those of a simple mechanical model in which one joint was moved by hand and the other was allowed to move under the influence of interaction torques alone.

The deficits in kinematic control and their dynamic basis appear similar to those seen in patients lacking proprioception because of large-fiber sensory neuropathy. As in AIP inactivation, these patients show increased hand-path curvature during reaching (Ghez et al. 1990; Gordon et al. 1995) and desynchronization of elbow and shoulder (Sainberg et al. 1995) resulting from a failure to take joint configuration or inertial interactions into account in feedforward control (Gordon et al. 1995; Sainberg et al. 1995). In both cases, dynamic analysis indicated that distal joint motion was effectively slaved to interaction torques developed by proximal joints. In the human, we have also shown that this feedforward control requires learning an internal model of inertial dynamics using proprioceptive information (Krakauer et al. 1999). Since the intermediate cerebellum and the AIP are important receiving areas for proprioceptive and other somatosensory inputs from the limb (Gellman et al. 1983; Gibson et al. 1987; Robinson et al. 1987; for review see Bloedel and Courville 1981), it appears plausible that the defect observed here reflects a similar abnormality. This suggests that these cerebellar circuits either perform the computations needed to establish internal models of limb biomechanics or that they store such models for use in controlling multijoint limb movement. This function of the AIP is consistent with the cerebellar modeling study of Schweighofer et al. (1998a,b) that examined control of a two-joint planar movement. In their model, the presence of feedforward (acceleration) control signals and proprioceptive feedback compensation did not correct for interaction torques and produced curved endpoint trajectories. When their model incorporated the learning of limb dynamical properties by a simulated cerebellum, interaction torques were adequately controlled and trajectories became straighter.

Independence of sensory-motor transformations underlying kinematic scaling and intersegmental dynamics

A striking feature of our results was that the scaling of paw velocity and the elbow motions responsible for the bulk of the lift phase (Martin et al. 1995) were preserved while control over intersegmental dynamics was disrupted by AIP inactivation. This can be interpreted in light of the results of recent studies of the sensorimotor transformations underlying reaching in humans and monkeys. Visual target information, initially encoded in retinotopic coordinates, is remapped into egocentric coordinates and then combined with hand position information to form a simplified, hand-centered vectorial plan of the intended movement trajectory as an extent and direction in extrinsic space (Flanders et al. 1992; Ghez et al. 1999). At this level, extent is specified by linearly scaling a stereotyped bell-shaped trajectory profile (Atkeson and Hollerbach 1985) to the desired target distance according to a learned scaling factor. Our results show that this process is not dependent on AIP.

For movement to occur however, the initial vectorial plan needs to be correctly transformed into intrinsic coordinates that specify the muscle forces and joint torques. This requires that muscle contractions at different joints be adapted to the motions that occur at all other joints. This was disrupted by AIP inactivation. As a result, movements were generated that, while scaled to the external target, did not incorporate the necessary compensation for inertial interactions that occurred within the limb. As a result, the movements were inaccurate.

The dynamic transformation compensating for inertial interactions, which failed during AIP inactivation, depends on an internal model of the limb, which may be adjusted through learning (Ghez et al. 1995; Sainberg et al. 1995; Shadmehr and Mussa-Ivaldi 1994). Recent psychophysical findings indicate that dynamic and vectorial transformations are represented and learned independently by the nervous system (Krakauer et al. 1999). Our findings suggest that the intermediate cerebellum plays a key role in using internal models of limb dynamics to plan accurate reaching movements.

APPENDIX

Equations of motion for a four-segment planar limb appear at the end of this appendix. They describe the relation between joint torque and joint motion at any given moment. The equation for each limb segment has the form $\Gamma = \{\text{term 1} + \text{term 2} + \ldots \text{term } n\} + G$ (shoulder, Γ_1; elbow, Γ_2; wrist, Γ_3; MCP, Γ_4). Γ is the torque that must have been acting at the joint to produce the motion described by the expression in curly brackets (G is the torque due to gravity, proportional to gravitational acceleration $g = 9.8$ m/s^2). Equivalently, the expression in curly brackets is an *inertial torque* and is the equal and opposite torque that must be overcome by muscle contraction (plus tendon stretch and ground reaction force if any) to produce the observed limb motion (d'Alembert's principle) (Cooper 1995). Since in this experiment we do not measure Γ directly but compute it from the fact that the right and left sides of the equation sum to zero, it corresponds to a residual term. In keeping with commonly-used terminology (e.g., Bastian et al. 1996; Smith and Zernicke 1987), we call Γ generalized muscle torque or, simply, *muscle torque*.

Each term of the expression for inertial torque consists of a coefficient (the complicated expression in square brackets) multiplied by a variable or variables (Θ) describing the limb motion. The joint-numbering conventions are the same as for Γ (Θ_1, shoulder; Θ_2, elbow; Θ_3, wrist; Θ_4, MCP). A single dot indicates an angular velocity and double dots indicate an angular acceleration. There are only three sorts of terms (Hollerbach and Flash 1982): dependent on acceleration, dependent on squared velocity (centrifugal), and dependent on the product of two velocities (Coriolis). The inertial torque also includes terms proportional to x and y components of linear acceleration of the shoulder, effectively lumping together the motion of all the joints proximal to the shoulder. In the present experiment, this component was small because linear motion of the shoulder was deliberately restricted. I_n is the moment of inertia of the segment distal to joint n, l_n is the length of that segment, and r_n is the distance from joint n to the segment's center of mass.

The terms in brackets are all functions of limb motion and could be expressed in terms of segment angles (that is, the angle of the limb segment relative to an absolute standard; Hoy et al. 1985) or joint angles (the angle between two adjacent limb segments) and the corresponding segment or joint angular velocities and accelerations. Because we view these terms as perturbing torques for which the nervous system must compensate, and because we hypothesize that the nervous system relies on proprioceptors for information about limb perturbations, we chose to

represent them in the coordinate system closest to what proprioceptors actually sense: joint angle. The choice of a joint-based coordinate system also affected the meaning of muscle torque. In a segment-based system, one would speak, for example, of forearm muscle torque produced by the combined action of elbow and wrist muscles. In the joint-based description, elbow muscle torque reflects elbow muscle contraction, which we feel is a more natural description. In this formulation, wrist muscles still contribute to the motion of the forearm, but they do so by producing wrist motion, which causes an interaction torque at the elbow.

The choice of joint-based equations resulted in a larger number of terms than if we had chosen to represent limb motion in terms of segment angles; this could have posed a problem for analysis if we had analyzed each term individually, but we instead grouped the terms into two components. Torques dependent only on the motion of the joint at which they act represent the passive inertial resistance of the limb to rotation of that joint; we called the sum of these torques *self torque.* The sum of torques dependent on the motion of other joints was called *interaction torque.*

$$
\begin{aligned}
\Gamma_1 = {} & \ddot{\Theta}_1 \left[\begin{array}{l} I_1 + I_2 + I_3 + I_4 + \\ m_1 r_1^2 + m_2(l_1^2 + r_2^2) + m_3(l_1^2 + l_2^2 + r_3^2) + m_4(l_1^2 + l_2^2 + l_3^2 + r_4^2) + \\ 2(m_2 r_2 l_1 + m_3 l_1 l_2 + m_4 l_1 l_2) \cos \Theta_2 + 2(m_3 r_3 l_1 + m_4 l_1 l_3) \cos (\Theta_2 + \Theta_3) + 2(m_4 r_4 l_1) \cos (\Theta_2 + \Theta_3 + \Theta_4) + \\ 2(m_3 r_3 l_2 + m_4 l_2 l_3) \cos \Theta_3 + 2(m_4 r_4 l_2) \cos (\Theta_3 + \Theta_4) + \\ 2(m_4 r_4 l_3) \cos \Theta_4 \end{array} \right] \\
& + \ddot{\Theta}_2 \left[\begin{array}{l} I_2 + I_3 + I_4 + \\ m_2(l_1^2 + r_2^2) + m_3(l_1^2 + l_2^2 + r_3^2) + m_4(l_1^2 + l_2^2 + l_3^2 + r_4^2) + \\ (m_2 r_2 l_1 + m_3 l_1 l_2 + m_4 l_1 l_2) \cos \Theta_2 + (m_3 r_3 l_1 + m_4 l_1 l_3) \cos (\Theta_2 + \Theta_3) + (m_4 r_4 l_1) \cos (\Theta_2 + \Theta_3 + \Theta_4) + \\ 2(m_3 r_3 l_2 + m_4 l_2 l_3) \cos \Theta_3 + 2(m_4 r_4 l_2) \cos (\Theta_3 + \Theta_4) + \\ 2(m_4 r_4 l_3) \cos \Theta_4 \end{array} \right] \\
& + \ddot{\Theta}_3 \left[\begin{array}{l} I_3 + I_4 + \\ m_3(l_1^2 + l_2^2 + r_3^2) + m_4(l_1^2 + l_2^2 + l_3^2 + r_4^2) + \\ (m_3 r_3 l_1 + m_4 l_1 l_3) \cos (\Theta_2 + \Theta_3) + (m_4 r_4 l_1) \cos (\Theta_2 + \Theta_3 + \Theta_4) + \\ (m_3 r_3 l_2 + m_4 l_2 l_3) \cos \Theta_3 + (m_4 r_4 l_2) \cos (\Theta_3 + \Theta_4) + \\ 2(m_4 r_4 l_3) \cos \Theta_4 \end{array} \right] \\
& + \ddot{\Theta}_4 \left[\begin{array}{l} I_4 + \\ m_4 r_4^2 + \\ (m_4 r_4 l_3) \cos \Theta_4 + (m_4 r_4 l_2) \cos (\Theta_3 + \Theta_4) + (m_4 r_4 l_1) \cos (\Theta_2 + \Theta_3 + \Theta_4) \end{array} \right] \\
& - \dot{\Theta}_2^2 [(m_2 r_2 l_1 + m_3 l_1 l_2 + m_4 l_1 l_2) \sin \Theta_2 + (m_3 r_3 l_1 + m_4 l_1 l_3) \sin (\Theta_2 + \Theta_3) + (m_4 r_4 l_1) \sin (\Theta_2 + \Theta_3 + \Theta_4)] \\
& - \dot{\Theta}_3^2 \left[\begin{array}{l} (m_3 r_3 l_1 + m_4 l_1 l_3) \sin (\Theta_2 + \Theta_3) + (m_4 r_4 l_1) \sin (\Theta_2 + \Theta_3 + \Theta_4) + \\ (m_3 r_3 l_2 + m_4 l_2 l_3) \sin \Theta_3 + (m_4 r_4 l_2) \sin (\Theta_3 + \Theta_4) \end{array} \right] \\
& - \dot{\Theta}_4^2 [(m_4 r_4 l_3) \sin \Theta_4 + (m_4 r_4 l_2) \sin (\Theta_3 + \Theta_4) + (m_4 r_4 l_1) \sin (\Theta_2 + \Theta_3 + \Theta_4)] \\
& - \dot{\Theta}_1 \dot{\Theta}_2 [2(m_2 r_2 l_1 + m_3 l_1 l_2 + m_4 l_1 l_2) \sin \Theta_2 + 2(m_3 r_3 l_1 + m_4 l_1 l_3) \sin (\Theta_2 + \Theta_3) + 2(m_4 r_4 l_1) \sin (\Theta_2 + \Theta_3 + \Theta_4)] \\
& - \dot{\Theta}_1 \dot{\Theta}_3 [2(m_3 r_3 l_2 + m_4 l_2 l_3) \sin \Theta_3 + 2(m_3 r_3 l_1 + m_4 l_1 l_3) \sin (\Theta_2 + \Theta_3) + 2(m_4 r_4 l_2) \sin (\Theta_3 + \Theta_4) + 2(m_4 r_4 l_1) \sin (\Theta_2 + \Theta_3 + \Theta_4)] \\
& - \dot{\Theta}_1 \dot{\Theta}_4 [2(m_4 r_4 l_3) \sin \Theta_4 + 2(m_4 r_4 l_2) \sin (\Theta_3 + \Theta_4) + 2(m_4 r_4 l_1) \sin (\Theta_2 + \Theta_3 + \Theta_4)] \\
& - \dot{\Theta}_2 \dot{\Theta}_3 [2(m_3 r_3 l_2 + m_4 l_2 l_3) \sin \Theta_3 + 2(m_3 r_3 l_1 + m_4 l_1 l_3) \sin (\Theta_2 + \Theta_3) + 2(m_4 r_4 l_2) \sin (\Theta_3 + \Theta_4) + 2(m_4 r_4 l_1) \sin (\Theta_2 + \Theta_3 + \Theta_4)] \\
& - \dot{\Theta}_2 \dot{\Theta}_4 [2(m_4 r_4 l_3) \sin \Theta_4 + 2(m_4 r_4 l_2) \sin (\Theta_3 + \Theta_4) + 2(m_4 r_4 l_1) \sin (\Theta_2 + \Theta_3 + \Theta_4)] \\
& - \dot{\Theta}_3 \dot{\Theta}_4 [2(m_4 r_4 l_3) \sin \Theta_4 + 2(m_4 r_4 l_2) \sin (\Theta_3 + \Theta_4) + 2(m_4 r_4 l_1) \sin (\Theta_2 + \Theta_3 + \Theta_4)] \\
& - \ddot{x} \left[\begin{array}{l} (m_1 r_1 + m_2 r_1 + m_3 r_1 + m_4 r_1) \sin \Theta_1 + (m_2 r_2 + m_3 r_2 + m_4 r_2) \sin (\Theta_1 + \Theta_2) + \\ (m_3 r_3 + m_4 r_3) \sin (\Theta_1 + \Theta_2 + \Theta_3) + (m_4 r_4) \sin (\Theta_1 + \Theta_2 + \Theta_3 + \Theta_4) \end{array} \right] \\
& - \ddot{y} \left[\begin{array}{l} (m_1 r_1 + m_2 r_1 + m_3 r_1 + m_4 r_1) \cos \Theta_1 + (m_2 r_2 + m_3 r_2 + m_4 r_2) \cos (\Theta_1 + \Theta_2) + \\ (m_3 r_3 + m_4 r_3) \cos (\Theta_1 + \Theta_2 + \Theta_3) + (m_4 r_4) \cos (\Theta_1 + \Theta_2 + \Theta_3 + \Theta_4) \end{array} \right] \\
\Gamma_2 = {} & \ddot{\Theta}_1 \left[\begin{array}{l} I_1 + I_3 + I_4 + \\ m_2 r_2^2 + m_3(l_2^2 + r_3^2) + m_4(l_2^2 + l_3^2 + r_4^2) + \\ (m_2 r_2 l_1 + m_3 l_2 l_1 + m_4 l_2 l_1) \cos \Theta_2 + (m_3 r_3 l_1 + m_4 l_3 l_1) \cos (\Theta_2 + \Theta_3) + (m_4 r_4 l_1) \cos (\Theta_2 + \Theta_3 + \Theta_4) + \\ 2(m_3 r_3 l_2 + m_4 l_3 l_2) \cos \Theta_3 + 2(m_4 r_4 l_2) \cos (\Theta_3 + \Theta_4) + \\ 2(m_4 r_4 l_3) \cos \Theta_4 \end{array} \right] \\
& + \ddot{\Theta}_2 \left[\begin{array}{l} I_2 + I_3 + I_4 + \\ m_2 r_2^2 + m_3(l_2^2 + r_3^2) + m_4(l_2^2 + l_3^2 + r_4^2) + \\ 2(m_3 r_3 l_2 + m_4 l_3 l_2) \cos \Theta_3 + 2(m_4 r_4 l_2) \cos (\Theta_3 + \Theta_4) + \\ 2(m_4 r_4 l_3) \cos \Theta_4 \end{array} \right]
\end{aligned}
$$

$$+ \ddot{\Theta}_3 \left[\begin{array}{l} I_3 + I_4 + \\ m_3 r_3^2 + m_4(l_3^2 + r_4^2) + \\ (m_3 r_3 l_2 + m_4 l_3 l_2) \cos \Theta_3 + (m_4 r_4 l_2) \cos (\Theta_3 + \Theta_4) + \\ 2(m_4 r_4 l_3) \cos \Theta_4 \end{array} \right]$$

$$- \ddot{\Theta}_4 \left[\begin{array}{l} I_4 + \\ m_4 r_4^2 + \\ (m_4 r_4 l_2) \cos (\Theta_3 + \Theta_4) + \\ (m_4 r_4 l_3) \cos \Theta_4 \end{array} \right]$$

$$+ \dot{\Theta}_1^2[(m_2 r_2 l_1 + m_3 l_2 l_1 + m_4 l_2 l_1) \sin \Theta_2 + (m_3 r_3 l_1 + m_4 l_2 l_1) \sin (\Theta_2 + \Theta_3) + (m_4 r_4 l_1) \sin (\Theta_2 + \Theta_3 + \Theta_4)]$$

$$- \dot{\Theta}_3^2[(m_3 r_3 l_2) \sin \Theta_3 + (m_4 r_4 l_2) \sin (\Theta_3 + \Theta_4)]$$

$$- \dot{\Theta}_4^2(m_4 r_4 l_3) \sin \Theta_4 + (m_4 r_4 l_2) \sin (\Theta_3 + \Theta_4)]$$

$$- \dot{\Theta}_1 \dot{\Theta}_3[2(m_3 r_3 l_2 + m_4 l_3 l_2) \sin \Theta_3 + 2(m_4 r_4 l_2) \sin (\Theta_3 + \Theta_4)]$$

$$- \dot{\Theta}_1 \dot{\Theta}_4[2(m_4 r_4 l_3) \sin \Theta_4 + 2(m_4 r_4 l_2) \sin (\Theta_3 + \Theta_4)]$$

$$- \dot{\Theta}_2 \dot{\Theta}_3[2(m_3 r_3 l_2 + m_4 l_3 l_2) \sin \Theta_3 + 2(m_4 r_4 l_2) \sin (\Theta_3 + \Theta_4)]$$

$$- \dot{\Theta}_2 \dot{\Theta}_4[2(m_4 r_4 l_3) \sin \Theta_4 + 2(m_4 r_4 l_2) \sin (\Theta_3 + \Theta_4)]$$

$$- \dot{\Theta}_3 \dot{\Theta}_4[2(m_4 r_4 l_3) \sin \Theta_4 + 2(m_4 r_4 l_2) \sin (\Theta_3 + \Theta_4)]$$

$$+ \ddot{x}[(m_2 r_2 + m_3 l_2 + m_4 l_2) \sin (\Theta_1 + \Theta_2) + (m_3 r_3 + m_4 l_3) \sin (\Theta_1 + \Theta_2 + \Theta_3) + (m_4 r_4) \sin (\Theta_1 + \Theta_2 + \Theta_3 + \Theta_4)]$$

$$+ \ddot{y}[(m_2 r_2 + m_3 l_2 + m_4 l_2) \cos (\Theta_1 + \Theta_2) + (m_3 r_3 + m_4 l_3) \cos (\Theta_1 + \Theta_2 + \Theta_3) + (m_4 r_4) \cos (\Theta_1 + \Theta_2 + \Theta_3 + \Theta_4)]$$

$$\Gamma_3 = \ddot{\Theta}_1 \left[\begin{array}{l} I_3 + I_4 + \\ m_3 r_3^2 + m_4(r_4 + l_3) + \\ (m_3 r_3 + m_4 l_3) \cos (\Theta_2 + \Theta_3) + (m_4 r_4 l_1) \cos (\Theta_2 + \Theta_3 + \Theta_4) + \\ (m_3 l_3 l_2) \cos \Theta_3 + (m_4 r_4 l_2) \cos (\Theta_3 + \Theta_4) \end{array} \right]$$

$$+ \ddot{\Theta}_2 \left[\begin{array}{l} I_3 + I_4 + \\ m_3 r_3 + m_4(r_4^2 + l_3^2) + \\ (m_3 r_3 l_2 + m_4 l_3 l_2) \cos \Theta_3 + (m_4 r_4 l_2) \cos (\Theta_3 + \Theta_4) + \\ 2(m_4 r_4 l_3) \cos \Theta_4 \end{array} \right]$$

$$+ \ddot{\Theta}_3 \left[\begin{array}{l} I_3 + I_4 + \\ m_3 r_3^2 + m_4(r_4^2 + l_3^2) + \\ 2(m_4 r_4 l_3) \cos \Theta_4 \end{array} \right]$$

$$+ \ddot{\Theta}_4 \left[\begin{array}{l} I_4 + \\ m_4 r_4^2 + \\ m_4 r_4 l_3) \cos \Theta_4 \end{array} \right]$$

$$+ \dot{\Theta}_1^2 \left[\begin{array}{l} (m_3 r_3 l_1 + m_4 l_3 l_1) \sin (\Theta_2 + \Theta_3) + (m_4 r_4 l_1) \sin (\Theta_2 + \Theta_3 + \Theta_4) + \\ (m_3 r_3 l_2 + m_4 l_3 l_2) \sin \Theta_3 + (m_4 r_4 l_2) \sin (\Theta_3 + \Theta_4) \end{array} \right]$$

$$+ \dot{\Theta}_2^2[(m_3 r_3 l_2 + m_4 l_3 l_2) \sin \Theta_3 + (m_4 r_4 l_2) \sin (\Theta_3 + \Theta_4)]$$

$$- \dot{\Theta}_4^2[(m_4 r_4 l_3) \sin \Theta_4]$$

$$+ \dot{\Theta}_1 \dot{\Theta}_2[2(m_3 r_3 l_2 + m_4 l_3 l_2) \sin \Theta_3 + 2(m_4 r_4 l_2) \sin (\Theta_3 + \Theta_4)]$$

$$- \dot{\Theta}_1 \dot{\Theta}_4[2(m_4 r_4 l_3) \sin \Theta_4]$$

$$+ \dot{\Theta}_2 \dot{\Theta}_4[2(m_4 r_4 l_3) \sin \Theta_4]$$

$$- \dot{\Theta}_3 \dot{\Theta}_4[2(m_4 r_4 l_3) \sin \Theta_4]$$

$$+ \ddot{x}[(m_3 r_3 + m_4 l_3) \sin (\Theta_1 + \Theta_2 + \Theta_3) + (m_4 r_4) \sin (\Theta_1 + \Theta_2 + \Theta_3 + \Theta_4)]$$

$$- \ddot{y}[(m_3 r_3 + m_4 l_3) \cos (\Theta_1 + \Theta_2 + \Theta_3) + (m_4 r_4) \cos (\Theta_1 + \Theta_2 + \Theta_3 + \Theta_4)]$$

$$\Gamma_4 = \ddot{\Theta}_1[I_4 + m_4 r_4^2 + m_4 r_4 l_3 \cos \Theta_4 + m_4 r_4 l_2 \cos (\Theta_3 + \Theta_4) + m_4 r_4 l_1 \cos (\Theta_2 + \Theta_3 + \Theta_4)]$$

$$+ \ddot{\Theta}_2[I_4 + m_4 r_4^2 + m_4 r_4 l_3 \cos \Theta_4 + m_4 r_4 l_3 \cos (\Theta_3 + \Theta_4)]$$

$$+ \ddot{\Theta}_3[I_4 + m_4 r_4^2 + m_4 r_4 l_3 \cos \Theta_4]$$

$$+ \ddot{\Theta}_4[I_4 + m_4 r_4^2]$$

$$+ \dot{\Theta}_1^2[m_4 r_4 l_3 \sin \Theta_4 + m_4 r_4 l_2 \sin (\Theta_3 + \Theta_4) + m_4 r_4 l_1 \sin (\Theta_2 + \Theta_3 + \Theta_4)]$$

$$+ \dot{\Theta}_2^2[m_4 r_4 l_3 \sin \Theta_4 + m_4 r_4 l_2 \sin (\Theta_3 + \Theta_4)]$$

$$+ \dot{\Theta}_3^2[m_4 r_4 l_3 \sin \Theta_4]$$

$$+ \dot{\Theta}_1\dot{\Theta}_2[2m_4r_4l_3 \sin \Theta_4 + 2m_4r_4l_2 \sin (\Theta_3 + \Theta_4)]$$

$$+ \dot{\Theta}_1\dot{\Theta}_3[2m_4r_4l_3 \sin \Theta_4]$$

$$+ \dot{\Theta}_2\dot{\Theta}_3[2m_4r_4l_3 \sin \Theta_4]$$

$$+ \ddot{x}[m_4r_4 \sin (\Theta_1 + \Theta_2 + \Theta_3 + \Theta_4)]$$

$$- \ddot{y}[m_4r_4 \cos (\Theta_1 + \Theta_2 + \Theta_3 + \Theta_4)]$$

We thank G. Johnson for construction of apparatus. We are grateful to Dr. Stephen Strain for assistance in deriving dynamic equations and to T. Hacking for expert technical assistance.

This research was supported by National Institute of Neurological Disorders and Stroke Grants NS-31391 to C. Ghez and NS-36865 to J. H. Martin, and Medical Scientist Training Program Grant 5T32-GM07367-20 to S. E. Cooper.

Present address of S. E. Cooper: Dept. of Neurology, Columbia University, 710 W. 168th St., New York, NY 10032.

REFERENCES

ANDERSON ME AND DEVITO JL. An analysis of potentially converging inputs to the rostral ventral thalamic nuclei of the cat. *Exp Brain Res* 68: 260–276, 1987.

ATKESON CG AND HOLLERBACH JM. Kinematic features of unrestrained vertical arm movements. *J Neurosci* 5: 2318–2330, 1985.

BASTIAN AJ, MARTIN TA, KEATING JG, AND THACH WT. Cerebellar ataxia: abnormal control of interaction torques across multiple joints. *J Neurophysiol* 76: 492–509, 1996.

BERMAN AL. *The Brain Stem of the Cat.* Madison, WI: University of Wisconsin, 1968, p. 1–175.

BERNTSON GG, PAULUCCI TS, AND TORELLO MW. An atlas of the deep cerebellar nuclei and subtentorial brainstem of the cat with compensation for skull size. *Brain Res Bull* 3: 475–492, 1978.

BLOEDEL JR AND COURVILLE J. Cerebellar afferent systems. In: *Handbook of Physiology, Neurophysiology,* edited by Brooks VB. Bethesda, MD: American Physiological Society, 1981, vol. II, p. 735–829.

BROOKS VB AND THACH WT. Cerebellar control of posture and movement. In: *Handbook of Physiology, Neurophysiology,* edited by Brookhart JM and Mountcastle VB. Bethesda, MD: American Physiological Society, 1981, vol. II, p. 877–946.

COOPER SE. *The Cerebellum and Interjoint Coordination: A Kinematic and Dynamic Analysis of an Accurate Multi-Joint Movement During Reversible Inactivation of the Cerebellar Nuclei.* New York: Columbia University, 1995, p. 158.

COOPER SE AND GHEZ C. Forelimb reaching in cats with lesions of the deep cerebellar nuclei: accuracy and interjoint coordination. *Soc Neurosci Abstr* 17: 1381, 1991.

FLANDERS M, HELMS TILLERY SI, AND SOECHTING JF. Early stages in a sensorimotor transformation. *Behav Brain Sci* 15: 309–362, 1992.

GELLMAN R, HOUK JC, AND GIBSON AR. Somatosensory properties of the inferior olive of the cat. *J Comp Neurol* 215: 228–243, 1983.

GHEZ C, COOPER SC, AND MARTIN J. Kinematic and dynamic factors in the coordination of prehension movements. In: *Hand and Brain: Neurophysiology and Psychology of Hand Movement,* edited by Haggard P, Flanagan R, and Wing W. Orlando, FL: Academic, 1996, p. 187–211.

GHEZ C, GORDON J, AND GHILARDI MF. Impairments of reaching movements in patients without proprioception. II. Effects of visual information on accuracy. *J Neurophysiol* 73: 361–372, 1995.

GHEZ C, GORDON J, GHILARDI M-F, CHRISTOKOS CN, AND COOPER SE. Roles of proprioceptive input in the programming of arm trajectories. *Cold Spring Harb Symp Quant Biol* 55: 837–847, 1990.

GHEZ C, KRAKAUER JW, SAINBURG RL, AND GHILARDI M-F. Spatial representations and internal models of limb dynamics in motor learning. In: *The New Cognitive Neurosciences,* edited by Gazzaniga MS. Cambridge, MA: MIT, 1999, p. 501–514.

GHEZ C AND VICARIO D. The control of rapid limb movement in the cat. I. Response latency. *Exp Brain Res* 33: 173–190, 1978.

GIBSON AR, ROBINSON FR, ALAM J, AND HOUK JC. Somatotopic alignment between climbing fiber input and nuclear output of the cat intermediate cerebellum. *J Comp Neurol* 260: 362–377, 1987.

GORDON J, GHILARDI MF, AND GHEZ C. Accuracy of planar reaching movements. I. Independence of direction and extent variability. *Exp Brain Res* 99: 97–111, 1994.

GORDON J, GHILARDI MF, AND GHEZ C. Impairments of reaching movements in patients without proprioception. I. Spatial errors. *J Neurophysiol* 73: 347–360, 1995.

HOLLERBACH JM AND FLASH T. Dynamic interactions between limb segments during planar arm movement. *Biol Cybern* 44: 67–77, 1982.

HOLMES G. The cerebellum of man. *Brain* 62: 1–30, 1939.

HOY MG AND ZERNICKE RF. Modulation of limb dynamics in the swing phase of locomotion. *J Biomech* 18: 49–60, 1985.

HOY MG, ZERNICKE RF, AND SMITH JL. Contrasting roles of inertial and muscle moments at knee and ankle during paw-shake response. *J Neurophysiol* 54: 1282–1294, 1985.

JAKOBSON LS AND GOODALE MA. Factors affecting higher-order movement planning: a kinematic analysis of human prehension. *Exp Brain Res* 86: 199–208, 1991.

JEANNEROD M. The timing of natural prehension movements. *J Motor Behav* 16: 235–254, 1984.

JÖRNTELL H AND EKEROT CF. Topographical organization of projections to cat motor cortex from nucleus interpositus anterior and forelimb skin. *J Physiol (Lond)* 514: 551–566, 1999.

KRAKAUER JW, GHILARDI MF, AND GHEZ C. Independent learning of internal models for kinematic and dynamic control of reaching. *Nat Neurosci* 2: 1026–1031, 1999.

LUCIANI L. *Human Physiology: Muscular and Nervous Systems.* London: MacMillan, 1915, vol III.

MARTIN JH, COOPER SC, AND GHEZ C. Kinematic analysis of reaching in the cat. *Exp Brain Res* 102: 379–392, 1995.

MARTIN JH, COOPER SE, HACKING A, AND GHEZ C. Differential effects of deep cerebellar nuclei inactivation on reaching and adaptive control. *J Neurophysiol* 83: 1886–1899, 2000.

MARTIN JH AND GHEZ C. Differential impairments in reaching and grasping produced by local inactivation within the forelimb representation of the motor cortex in the cat. *Exp Brain Res* 94: 429–443, 1993.

MARTIN JH AND GHEZ C. Pharmacological inactivation in the analysis of the central control of movement. *J Neurosci Meth* 86: 145–159, 1999.

MIALL RC. The cerebellum, predictive control and motor coordination. *Novartis Found Symp* 218: 272–284, 1998.

MILAK MS, SHIMANSKY Y, BRACHA V, AND BLOEDEL JR. Effects of inactivating individual cerebellar nuclei on the performance and retention of an operantly conditioned forelimb movement. *J Neurophysiol* 78: 939–959, 1997.

MORASSO P. Spatial control of arm movements. *Exp Brain Res* 42: 223–227, 1981.

PERFILIEV S AND PETTERSSON LG. Characteristics of target-reaching in cats. III. Lifting and protraction with an obstacle in the movement path and after its removal. *Exp Brain Res* 120: 510–518, 1998.

PETTERSSON LG, LUNDBERG A, ALSTERMARK B, ISA T, AND TANTISIRA B. Effect of spinal cord lesions on forelimb target-reaching and on visually guided switching of target-reaching in the cat. *Neurosci Res* 29: 241–256, 1997.

ROBINSON FR, HOUK JC, AND GIBSON AR. Limb specific connections of the cat magnocellular red nucleus. *J Comp Neurol* 257: 553–577, 1987.

SAINBURG RL, GHILARDI F, POIZNER H, AND GHEZ C. Control of limb dynamics in normal subjects and patients without proprioception. *J Neurophysiol* 73: 820–835, 1995.

SCHWEIGHOFER N, ARBIB MA, AND KAWATO M. Role of the cerebellum in reaching movements in humans. I. Distributed inverse dynamics control. *Eur J Neurosci* 10: 86–94, 1998.

SCHWEIGHOFER N, SPOELSTRA J, ARBIB MA, AND KAWATO M. Role of the cerebellum in reaching movements in humans. II. A neural model of the intermediate cerebellum. *Eur J Neurosci* 10: 95–105, 1998.

SHADMEHR R AND MUSSA-IVALDI FA. Adaptive representation of dynamics during learning of a motor task. *J Neurosci* 14: 3208–3224, 1994.

SMITH JL AND ZERNICKE RF. Predictions for neural control based on limb dynamics. *Trends Neurosci* 10: 123–128, 1987.

THACH WT, GOODKIN HP, AND KEATING JG. The cerebellum and the adaptive coordination of movement. *Ann Rev Neurosci* 15: 403–442, 1992.

TROTT JR AND ARMSTRONG DM. The cerebellar corticonuclear projection from lobule Vb/c of the cat anterior lobe: a combined electrophysiological and autoradiographic study. *Exp Brain Res* 66: 318–338, 1987.

WOLPERT DM, GHAHRAMANI Z, AND JORDAN MI. An internal model for sensorimotor integration. *Science* 269: 1880–1882, 1995.